


**Coherent control of 40-THz optical phonons in diamond using femtosecond optical pulses**Tetsuya Kimata <sup>1,2,\*</sup>, Kazuma Yoda,<sup>1,2</sup> Hana Matsumoto,<sup>1,2</sup> Hiroyuki Tanabe,<sup>1,2</sup> Fujio Minami,<sup>1,3</sup> Yosuke Kayanuma,<sup>1,4</sup> and Kazutaka G. Nakamura<sup>1,2,†</sup><sup>1</sup>*Laboratory for Materials and Structures, Institute for Innovative Research, Tokyo Institute of Technology, 4259 Nagatsuta, Yokohama 226-8503, Japan*<sup>2</sup>*Department of Materials Science and Engineering, Tokyo Institute of Technology, 4259 Nagatsuta, Yokohama 226-8503, Japan*<sup>3</sup>*Department of Physics, Yokohama National University, 79-5 Tokiwadai, Yokohama 240-8501, Japan*<sup>4</sup>*Graduate School of Sciences, Osaka Prefecture University, 1-1 Gakuen-cho, Sakai 599-8531, Japan*

(Received 1 January 2020; accepted 14 April 2020; published 4 May 2020)

A theory of the coherent control of optical phonons by double-pulse excitation was modified for the calculation of a large detuning case such as diamond; we calculated the amplitude of the optical phonons without using a rotating-wave approximation. Additionally, we took the frequency chirping and non-Gaussian pulse shape into consideration. The coherent control of the amplitude of 40 THz optical phonons in diamond was demonstrated by using a pair of infrared pulses at a pump-pump delay between  $-10$  and  $120$  fs, and analyzed by using the modified theory.

DOI: [10.1103/PhysRevB.101.174301](https://doi.org/10.1103/PhysRevB.101.174301)**I. INTRODUCTION**

Coherent control is a technique to manipulate quantum states in matter using optical pulses [1–3] and applied to electronic states, spins, molecular vibrations, and phonons [4–12]. The coherent control of optical phonons has been widely achieved in various materials such as semiconductors, semimetals, superconductors, topological materials, strongly correlated materials, and dielectric materials [13–19]. Recently, a theory of the coherent control of optical phonons by double-pulse excitation has been developed based on a simple quantum mechanical model with two electronic bands and shifted harmonic oscillators [20,21]. We demonstrated the coherent control experiment on the optical phonons in a single crystal of diamond and analyzed the data by using the developed theory [22].

The optical phonon in diamond has a high frequency (approximately 40 THz) and is expected to be used as a qubit operating at room temperature [23–26]. Coherent optical phonons in diamond have been studied using femtosecond optical pulses and their generation mechanism has also been discussed with quantum mechanical calculations [21,22,27–30]. We have demonstrated the coherent control of the amplitude and phase of the coherent optical-phonon oscillation in diamond using a pair of sub-10-fs infrared pulses at delays between 230 and 270 fs, in which two pump pulses were well separated [22]. The observed behavior of the amplitude and phase were well reproduced as a simple interference between two phonon oscillations by the developed theory. However, it is very important to study the time region around

where two optical pulses are overlapped, because a sign of interference in electron-phonon coupled states [31–36], which could not be reproduced by classical mechanics, appears in this region. The difference in the interference patterns for the impulsive absorption process and the impulsive stimulated Raman scattering (ISRS) process has been clearly shown in a GaAs crystal [13]. In order to study large detuning conditions and a non-Gaussian pulse shape, the modification of the theory should be required.

In the present paper, we modify the theory in order to calculate the large detuning case without using a rotating-wave approximation and take the frequency chirping and non-Gaussian pulse shape into consideration. We perform the coherent control of amplitude of the 40 THz optical phonons in diamond by using a pair of infrared pulses at pump-pump delays between  $-10$  and  $120$  fs, and analyze the experimental result using the theory based on the quantum mechanical model.

**II. THEORETICAL MODEL**

Here, we consider coherent phonon generation in diamond with a sub-10-fs infrared pulse. The coherent optical phonons should be excited by the ISRS process at an off-resonant condition because the energy of the optical pulses (around 1.5 eV) was well below the direct band gap (7.3 eV) of diamond [37,38]. It should be noted that we do not use a Gaussian pulse shape and a usual rotating-wave approximation, because the detuning is quite large. A frequency chirping in the sub-10-fs pulse is also included.

We calculated the generation of the coherent phonons using a simple model with two electronic levels and shifted harmonic oscillators. We used a model Hamiltonian of the electron-phonon system as

$$H = \hbar\omega b^\dagger b |g\rangle \langle g| + [\epsilon + \hbar\omega b^\dagger b + \alpha\hbar\omega(b + b^\dagger)] |e\rangle \langle e|, \quad (1)$$

\*Also at: Ground Systems Research Center, Ministry of Defense (ATLA), 2-9-54 Fuchinobe, Sagamihara 252-0206, Japan; kimata.t.aa@m.titech.ac.jp

†nakamura.k.ai@m.titech.ac.jp

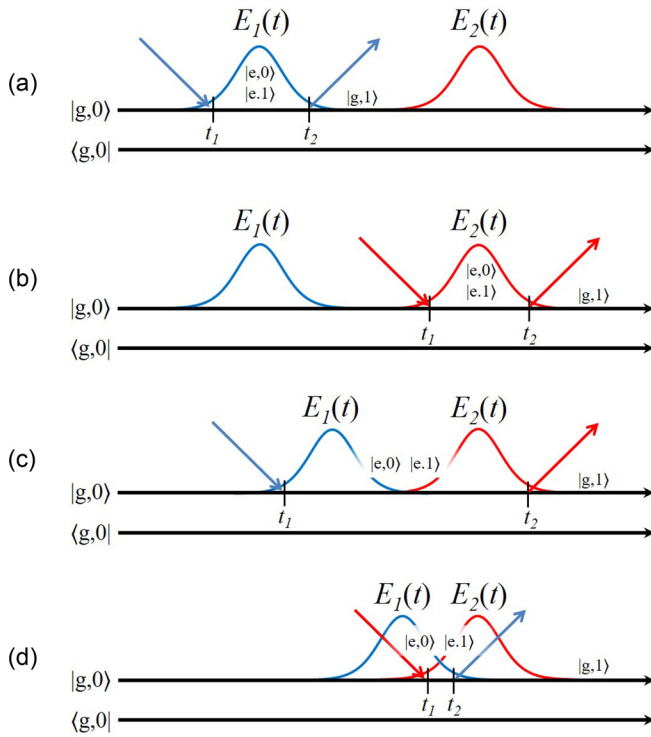


FIG. 1. Diagram of the ISRS paths. Transition occurs by only (a) pump 1 or (b) pump 2. (c) and (d) represent the transition occurring by both pumps 1 and 2. Time flows from the left to the right. The upper part of the diagram shows an envelope of the optical pulse. An interaction between the optical pulse and the system occurs at times  $t_1$  and  $t_2$ .

where  $\omega$  is the phonon frequency,  $\epsilon$  is the excitation energy, and  $\alpha$  represents the electron-phonon coupling.  $|g\rangle$  and  $|e\rangle$  denote the electronic ground and excited states, respectively.  $b^\dagger$  and  $b$  denote the creation and annihilation operators for the phonon. The interaction Hamiltonian with the optical pulse is given by

$$H_I = \mu E(t) (|e\rangle \langle g| + |g\rangle \langle e|), \quad (2)$$

where  $\mu$  is the transition dipole moment and  $E(t)$  is the electric field of the pulse. We used a density operator formalism and the second-order perturbation, which is described in previous papers [20,39].

Figure 1 shows the double-side Feynman diagrams for ISRS paths on the double-pulse excitation [13].  $E_1(t)$  and  $E_2(t)$  are the electric fields of pumps 1 and 2. An interaction between the optical pulse and the system occurs at times  $t_1$  and  $t_2$ . The first diagram [Fig. 1(a)] indicates path A, in which the phonons are generated by only pump 1; the electronic excitation and deexcitation occur within the pulse. In a similar way, the phonons are generated by only pump 2, which is path B and shown in the second diagram [Fig. 1(b)]. Figures 1(c) and 1(d) show paths C and D in which the phonons are excited by both pumps 1 and 2. The phonon excitation and deexcitation are induced by pumps 1 and 2, respectively, in path C and vice versa in path D.

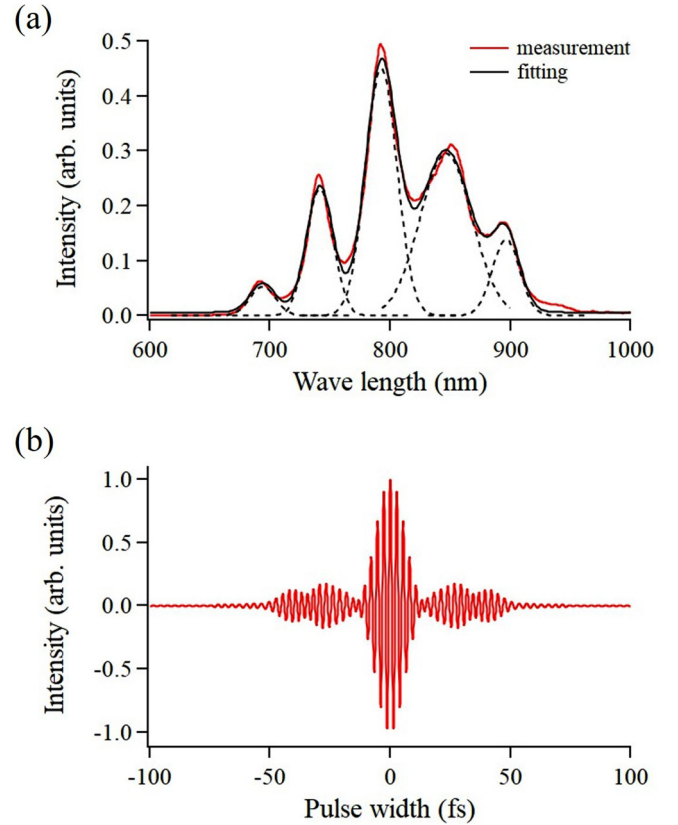


FIG. 2. (a) The measured spectrum of the ultrafast laser pulse (red) and the curve fitting with five Gaussian pulses (black). The dashed curves are each Gaussian pulses. (b) Electric field intensity generated from the five Gaussian curves. Obtained parameters for five Gaussian pulses are listed in the text.

By using the second-order perturbation, the density operator for all paths,  $\rho(t)$ , is obtained as

$$\rho(t) = \alpha \left( \frac{\mu}{\hbar} \right)^2 e^{-i\omega t} \sum_{j=1}^2 \sum_{k=1}^2 \int_{-\infty}^t dt_2 \int_{-\infty}^{t_2} dt_1 E_j(t_1) E_k(t_2) \times e^{-\frac{i}{\hbar} \epsilon (t_2 - t_1)} (e^{i\omega t_1} - e^{i\omega t_2}) |g, 1\rangle \langle g, 0| + \text{H.c.}, \quad (3)$$

where  $|g, 1\rangle$  and  $|g, 0\rangle$  indicate the state vector for the electronic ground state with a one-phonon state and that with a zero-phonon state, respectively. It should be noted that time  $t$  should be enough after the irradiation of pump 2. Details for the calculation of the density operator are described elsewhere [13,39]. We describe details of the frequency chirping and non-Gaussian pulse shape in the Discussion section below.

### III. EXPERIMENT

#### A. Measurement setup

Coherent optical phonons were investigated using a pump-probe-type transient-transmission measurement with two pump pulses. The used laser was a Ti:sapphire oscillator (FEMTOLASERS, Rainbow) operating with a repetition rate of 75 MHz. Figure 2(a) shows the spectrum measured immediately behind the output port, which has peaks at 694, 742, 792, 846, and 896 nm, measured using a USB spectrometer

(OceanOptics, USB2000). Figure 2(b) shows the pulse waveform generated by the Fourier transformation of five Gaussian curves. The pulse width was estimated to be 8.3 fs at full width at half maximum by using the frequency-resolved autocorrelation measurement (FEMTOLASERS: Femtometer).

The output from the Ti:sapphire oscillator was introduced to compensate the group-velocity dispersion using a pair of chirp mirrors and divided into two pulses by a beam splitter. One was used as a pump pulse and the other was used as a probe pulse. The pump pulse was introduced to a scan-delay unit operating at 20 Hz in order to control a delay ( $t$ ) between the pump and probe pulses. The pump pulse is introduced to a home-made Michelson-type interferometer [40] to produce a pair of pump pulses (pumps 1 and 2). One optical arm of the interferometer was equipped with an automatic positioning stage (Sigma Tech Co. Ltd., FS-1050UPX), which moves with a minimum step of 1 nm. The delay between pumps 1 and 2,  $\tau$  (fs), was controlled by the stage of the Michelson interferometer in 0.5-fs steps. The optical interference of the pump-pump delay was detected by a photodiode (PD1).

The probe pulse was picked up by a 95:5 beam splitter to measure the reference beam intensity at a photodiode (PD2). Thereafter, both pump and probe pulses were focused on the sample by using an off-axis parabolic mirror. The transmitted pulse from the sample was detected with a photodiode (PD3). By applying the opposite bias voltages to PD2 and PD3, we set the balanced detection before the experiment. Its differential signal, amplified with a low-noise current amplifier (Stanford Research Systems, SR570), was measured by a digital oscilloscope (Iwatsu, DS5534). To reduce the statistical error, 32 000 signals were averaged and taken as the measured value. By converting the temporal motion of the scan delay unit to the pump-probe pulse duration, the temporal evolution of the transmittance change  $\Delta T/T_0$  was obtained. Here, we used the heterodyne detection technique. The powers of pumps 1 and 2 and the probe were 21.2, 21.3, and 3.1 mW, respectively.

The sample used was a single crystal of diamond with a [100] crystal plane, which was fabricated by chemical vapor deposition and obtained from the EPD Corporation. The type of diamond was intermediate between Ib and IIa and its size was  $5 \times 5 \times 0.7 \text{ mm}^3$ . The polarization of the pump and probe pulses were set along the [110] and  $[-110]$  axes, respectively.

## B. Measurement result

Figure 3 is a two-dimensional map of the transient transmittance change  $\Delta T/T_0$  as a function of the pump 1–probe delay ( $t$ , horizontal axis) and pump 1–pump 2 delay ( $\tau$ , vertical axis). At a fixed pump 1–pump 2 delay ( $\tau$ ),  $\Delta T/T_0$  shows a sharp peak at delay zero between the pump and probe and a successive oscillation with a frequency of  $39.9 \pm 0.05$  THz, which have been reported in a previous paper [22]. The oscillation is assigned to the optical phonons in diamond. On the other hand, at a fixed pump-probe delay ( $t$ ),  $\Delta T/T_0$  shows a rapid oscillation (approximately 380 THz) in addition to the oscillation due to the optical phonon (approximately 40 THz).

The Fourier transformation was performed between 0.5 and  $< 1.5$  ps along the pump-probe delay after the irradiation

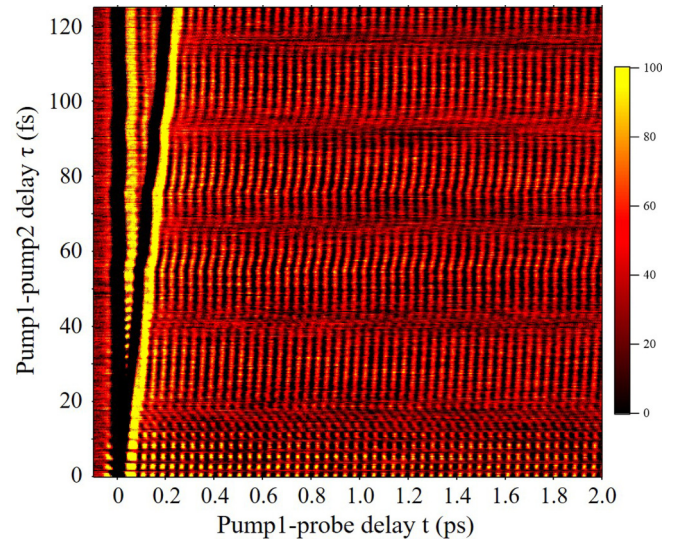


FIG. 3. Two-dimensional image map of the change in transition intensity with the pump 1–probe delay ( $t$ ) and pump 1–pump 2 delay ( $\tau$ ).

of pump 2 at the each pump-pump delay. The optical-phonon amplitude was obtained by integration of the Fourier-transformed data between 37.5 and 42.5 THz, and then plotted against the pump-pump delay  $\tau$  in Fig. 4(a). Figure 4(a) shows slow and fast oscillations, with an oscillational period of approximately 25 and 2.7 fs, respectively. The slow oscillation with a period of approximately 25 fs is observed at the pump-pump delay  $\tau > 15$  fs. This oscillation is consistent with the oscillating function in the range of the pump-pump

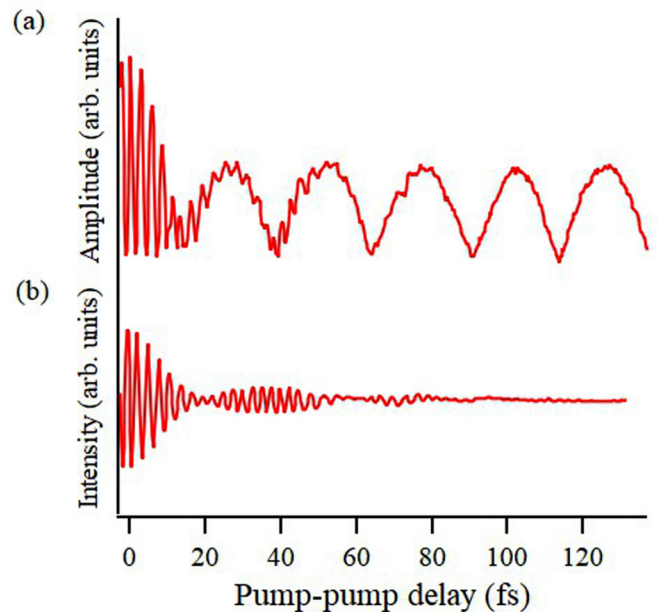


FIG. 4. The amplitude of (a) the controlled oscillation after pump 2 and (b) the optical interference against the pump-pump delay ( $\tau$ ). The amplitude is normalized using that obtained after excitation after only pump 1; oscillation between pump 1 and pump 2 irradiation timing.

delay between 230 and 270 fs in a previous study [22]. The amplitude is enhanced or suppressed at the timing of the pump-pump delay which matches the integer or half-integer multiple of the phonon oscillation period. This is due to the constructive or destructive interference of the coherent phonons. On the other hand, a rapid oscillation with a period of approximately 2.7 fs is observed at the pump-pump delay  $\tau < 15$  fs. This oscillation continues on the oscillating function of the constructive and destructive interference of coherent phonons until approximately 80 fs. The rapid oscillation would be originated by the optical interference of the dual pulses because of the influence of optical interference detected by PD1 [Fig. 4(b)] that appeared in Fig. 4(a).

#### IV. DISCUSSION

In the calculation, we used an optical pulse composed of five Gaussian pulses,

$$E_1(t) = \sum_{k=1}^5 E_k \exp\left(-\frac{t^2}{\sigma_k^2}\right) \cos[2\pi(\Omega_k + \theta t)t], \quad (4)$$

where  $E_k$ ,  $\Omega_k$ , and  $\sigma_k$  are the ratio of electric field strengths, the optical frequency, and the pulse width of each component. The parameters were determined by curve fitting of the measured spectrum with five Gaussian-shaped spectra. The fitted spectrum is shown in Fig. 2(a). The obtained parameters are  $(E_k, \Omega_k[1/\text{fs}], \sigma_k[1/\text{fs}]) = (0.045, 0.432, 0.035), (0.197, 0.405, 0.032), (0.385, 0.379, 0.033), (0.253, 0.354, 0.048),$  and  $(0.119, 0.335, 0.023)$ .  $\theta$  is the linear chirp rating. The electric field of pump 2 is defined as  $E_2(t) = E_1(t - \tau)$ , where  $\tau$  is a delay between pumps 1 and 2. In order to reproduce the actual pulse envelope,  $\theta$  is set to  $5 \times 10^{-4}$  ( $\text{fs}^{-2}$ ) by comparing the first-order optical interference derived from the electric field of the two pump pulses with the detected optical interference [Fig. 4(b)].

The mean value of the phonon coordinate is obtained by  $\langle Q(t) \rangle = \text{Tr}\{Q\rho(t)\}$ , where  $Q \equiv \sqrt{\hbar/2\omega}(b + b^\dagger)$  and Tr indicates that the trace should be taken over the electronic and phonon variables. In this study, the mean value was estimated by numeric calculation; the rotating-wave approximation is not applied due to the large detuning condition.

The calculated phonon amplitude for all paths shown in Fig. 5(b) represents well the experimental data [Fig. 5(a)]. The rapid oscillation with a period of approximately 2.7 fs at the pump-pump delay  $\tau < 15$  fs is caused by the optical interference, which is represented by paths C and D. This interference pattern corresponds well to the optical interference [shown in Fig. 4(b)], and the electronic-coherence effect, which was reported in the coherent-control experiments on GaAs at resonance conditions [39], has not been observed. On the other hand, the slow oscillation with a period of approximately 25 fs is caused by phonon interference, which is due to paths A and B. In fact, the calculated phonon amplitude via paths A and B shows only the slow oscillation as shown in Fig. 5(c). As

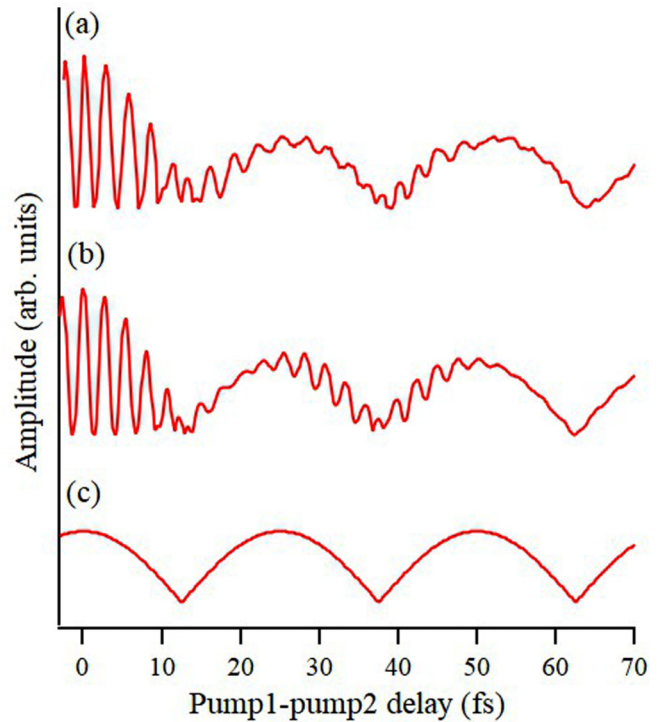


FIG. 5. (a) The measured amplitude of the controlled oscillation after pump 2 on the pulse overlap region. (b) The calculated phonon amplitude for all paths. (c) The calculated phonon amplitude for paths A and B.

already reported [22], the phonon amplitude after the second pump pulse irradiation is a sum of two sinusoidal functions induced by each pulse.

#### V. CONCLUSIONS

In order to calculate the large detuning case such as diamond crystal, we modified the theory without using a rotating-wave approximation. In addition, we take the frequency chirping and non-Gaussian pulse shape into consideration. The coherent control of the amplitude of 40 THz optical phonons in diamond was demonstrated by using a pair of infrared pulses at a pump-pump delay between  $-10$  and  $120$  fs, and analyzed by using the modified theory. As a result, the modified theory reproduced well the experimental data.

#### ACKNOWLEDGMENTS

The authors thank Professor Yutaka Shikano of Keio University and Riho Tanaka of Tokyo Tech for their efforts in the early stages of this work. This work was supported in part by JSPS KAKENHI Grants No. 15K13377, No. 17K19051, No. 17H02797, No. 19K03696, and No. 19K22141, Collaborative Research Project of Laboratory for Materials and Structures, Institute of Innovative Research, Tokyo Institute of Technology.

[1] P. Brumer and M. Shapiro, *Chem. Phys. Lett.* **126**, 541 (1986).

[2] S. A. Rice, D. J. Tannor, and R. Kosloff, *J. Chem. Soc., Faraday Trans.* **82**, 2423 (1986).

- [3] N. F. Scherer, R. J. Carlson, A. Matro, M. Du, A. J. Ruggiero, V. Romero-Rochin, J. A. Cina, G. R. Fleming, and S. A. Rice, *J. Chem. Phys.* **95**, 1487 (1991).
- [4] R. Unanyan, M. Fleischhauer, B. W. Shore, and K. Bergmann, *Opt. Commun.* **155**, 144 (1998).
- [5] T. C. Weinacht, J. Ahn, and P. H. Bucksbaum, *Nature (London)* **397**, 233 (1999).
- [6] D. Meshulach and Y. Silberberg, *Nature (London)* **396**, 239 (1998).
- [7] K. Ohmori, H. Katsuki, H. Chiba, M. Honda, Y. Hagihara, K. Fujiwara, Y. Sato, and K. Ueda, *Phys. Rev. Lett.* **96**, 093002 (2006).
- [8] H. Katsuki, H. Chiba, B. Girard, C. Meier, and K. Ohmori, *Science* **311**, 1589 (2006).
- [9] M. P. A. Branderhorst, P. Londero, P. Wasylczyk, C. Brif, R. L. Kosut, H. Rabitz, and I. A. Walmsley, *Science* **320**, 638 (2008).
- [10] K. Ohmori, *Annu. Rev. Phys. Chem.* **60**, 487 (2009).
- [11] A. Noguchi, Y. Shikano, K. Toyoda, and S. Urabe, *Nat. Commun.* **5**, 3868 (2014).
- [12] G. Higgins, F. Pokorny, C. Zhang, Q. Bodart, and M. Hennrich, *Phys. Rev. Lett.* **119**, 220501 (2017).
- [13] K. G. Nakamura, K. Yokota, Y. Okuda, R. Kase, T. Kitashima, Y. Mishima, Y. Shikano, and Y. Kayanuma, *Phys. Rev. B* **99**, 180301(R) (2019).
- [14] T. Dekorsy, W. Kütt, T. Pfeifer, and H. Kurz, *Europhys. Lett.* **23**, 223 (1993).
- [15] M. Hase, K. Mizoguchi, H. Harima, S. Nakashima, M. Tani, K. Sakai, and M. Hangyo, *Appl. Phys. Lett.* **69**, 2474 (1996).
- [16] Y.-H. Cheng, F. Y. Gao, S. W. Teitelbaum, and K. A. Nelson, *Phys. Rev. B* **96**, 134302 (2017).
- [17] F. Sun, Q. Wu, Y. L. Wu, H. Zhao, C. J. Yi, Y. C. Tian, H. W. Liu, Y. G. Shi, H. Ding, X. Dai, P. Richard, and J. Zhao, *Phys. Rev. B* **95**, 235108 (2017).
- [18] L. L. Hu, M. Yang, Y. L. Wu, Q. Wu, H. Zhao, F. Sun, W. Wang, R. He, S. L. He, H. Zhang, R. J. Huang, L. F. Li, Y. G. Shi, and J. Zhao, *Phys. Rev. B* **99**, 094307 (2019).
- [19] H. Mashiko, Y. Chisuga, I. Katayama, K. Oguri, H. Masuda, J. Takeda, and H. Gotoh, *Nat. Commun.* **9**, 1468 (2018).
- [20] K. G. Nakamura, Y. Shikano, and Y. Kayanuma, *Phys. Rev. B* **92**, 144304 (2015).
- [21] K. G. Nakamura, K. Ohya, H. Takahashi, T. Tsuruta, H. Sasaki, S. I. Uozumi, K. Norimatsu, M. Kitajima, Y. Shikano, and Y. Kayanuma, *Phys. Rev. B* **94**, 024303 (2016).
- [22] H. Sasaki, R. Tanaka, Y. Okano, F. Minami, Y. Kayanuma, Y. Shikano, and K. G. Nakamura, *Sci. Rep.* **8**, 9609 (2018).
- [23] K. C. Lee, M. R. Sprague, B. J. Sussman, J. Nunn, N. K. Langford, X.-M. Jin, T. Champion, P. Michelberger, K. F. Reim, D. England, D. Jaksch, and I. A. Walmsley, *Science* **334**, 1253 (2011).
- [24] K. C. Lee, B. J. Sussman, M. R. Sprague, P. Michelberger, K. F. Reim, J. Nunn, N. K. Langford, P. J. Bustard, D. Jaksch, and I. A. Walmsley, *Nat. Photonics* **6**, 41 (2012).
- [25] D. G. England, P. J. Bustard, J. Nunn, R. Lausten, and B. J. Sussman, *Phys. Rev. Lett.* **111**, 243601 (2013).
- [26] D. G. England, K. A. G. Fisher, J.-P. W. MacLean, P. J. Bustard, R. Lausten, K. J. Resch, and B. J. Sussman, *Phys. Rev. Lett.* **114**, 053602 (2015).
- [27] K. Ishioka, M. Hase, M. Kitajima, and H. Petek, *Appl. Phys. Lett.* **89**, 231916 (2006).
- [28] M. Zakerstein, M. Kozák, F. Trojánek, and P. Malý, *Diamond Relat. Matter.* **90**, 202 (2018).
- [29] M. Zakerstein, F. Trojánek, B. Rezek, Z. Šobáň, M. Kozák, and P. Malý, *Appl. Phys. Lett.* **115**, 161104 (2019).
- [30] A. Yamada and K. Yabana, *Phys. Rev. B* **99**, 245103 (2019).
- [31] J. Shah, in *Ultrafast Spectroscopy of Semiconductors and Semiconductor Nanostructures*, Springer Series in Solid-State Sciences Vol. 115 (Springer, Berlin, 1996).
- [32] A. P. Heberle, J. J. Baumberg, and K. Köhler, *Phys. Rev. Lett.* **75**, 2598 (1995).
- [33] M. U. Wehner, M. H. Ulm, D. S. Chemla, and M. Wegener, *Phys. Rev. Lett.* **80**, 1992 (1998).
- [34] M. Gurioli, F. Bogani, S. Ceccherini, and M. Colocci, *Phys. Rev. Lett.* **78**, 3205 (1997).
- [35] M. Wegener, *J. Lumin.* **87-89**, 20 (2000).
- [36] V. M. Axt and T. Kuhn, *Rep. Prog. Phys.* **67**, 433 (2004).
- [37] W. Saslow, T. K. Bergstresser, and M. L. Cohen, *Phys. Rev. Lett.* **16**, 354 (1966).
- [38] R. P. Mildren, in *Optical Engineering of Diamonds*, edited by R. P. Mildren and J. R. Rabeau (Wiley-VCH, Weinheim, 2013), pp. 1–34.
- [39] K. Nakamura, in *Quantum Phononics*, Springer Tracts in Modern Physics Vol. 282 (Springer, Berlin, 2019).
- [40] S. Hayashi, K. Kato, K. Norimatsu, M. Hada, Y. Kayanuma, and K. G. Nakamura, *Sci. Rep.* **4**, 4456 (2014).